

Layering transitions in superfluid helium adsorbed on a carbon nanotube mechanical resonator

Adrien Noury,^{1,*} Jorge Vergara-Cruz,¹ Pascal Morfin,² Bernard Plaçais,²
Maria C. Gordillo,³ Jordi Boronat,⁴ Sébastien Balibar,² and Adrian Bachtold¹

¹*ICFO - Institut De Ciències Fotoniques,
The Barcelona Institute of Science and Technology Mediterranean Technology Park,
08860 Castelldefels (Barcelona), Spain*

²*Laboratoire de Physique de l'École normale supérieure,
ENS, Université PSL, CNRS, Sorbonne Université,
Université Paris-Diderot, Sorbonne Paris Cité, Paris, France*

³*Departamento de Sistemas Físicos, Químicos y Naturales,
Universidad Pablo de Olavide Carretera de Utrera, km 1, E-41013 Sevilla, Spain*

⁴*Departament de Física, Universitat Politècnica de
Catalunya B4-B5 Campus Nord, 08034 Barcelona, Spain*

Abstract

Helium is recognized as a model system for the study of phase transitions. Of particular interest is the superfluid phase in two dimensions. We report measurements on superfluid helium films adsorbed on the surface of a suspended carbon nanotube. We measure the mechanical vibrations of the nanotube to probe the adsorbed helium film. We demonstrate the formation of helium layers up to five atoms thickness. Upon increasing the vapour pressure, we observe layer-by-layer growth with discontinuities in both the number of adsorbed atoms and the speed of sound in the adsorbed film. These hitherto unobserved discontinuities point to a series of first-order layering transitions. Our results show that helium multilayers adsorbed on a nanotube are of unprecedented quality compared to previous works. They pave the way to new studies of quantized superfluid vortex dynamics on cylindrical surfaces, of the Berezinskii-Kosterlitz-Thouless phase transition in this new geometry, perhaps also to supersolidity in crystalline single layers as predicted in quantum Monte Carlo calculations.

*Present address: Laboratoire Charles Coulomb (L2C), Univ Montpellier, CNRS, Montpellier, France

When exposing graphite to a helium vapor at low temperature, a helium film forms on the graphite surface. Several experiments have shown that the thickness of this film grows layer by layer as a function of the vapor pressure. These layers are one atom thick [1–5], and there are successive “layering transitions” between layers n and $n+1$. Clements et al. [6, 7] had predicted that the layering transitions are first order transitions, meaning that the coverage should show a series of sharp discontinuities as a function of the helium pressure. However, such discontinuities could not be observed, probably because previous techniques required large surface areas, which were obtained e.g. by chemically exfoliating graphite and by subsequently pressing the material into sheets. As a result, the substrate surface was made of small crystalline platelets of $\sim (10\text{nm})^2$ area [4] and probably contained a sizeable amount of defects including wedges where liquid helium could accumulate. Despite the modest quality of these surfaces, evidences for layer-by-layer growth were reported but without any visible discontinuities [1, 4, 5, 8, 9].

By studying the mechanical resonance of a single wall carbon nanotube (NT) we have observed discontinuities in the adsorbed mass as a function of the injection of helium atoms and demonstrated for the first time that the layering transitions are indeed first order. A carbon nanotube is an excellent substrate, since the crystalline quality is high, and such nanotubes can be made free of adsorbed contamination [10]. Our results prove the very high quality of carbon nanotubes as potential substrates for new original studies like quantized superfluid vortex dynamics on cylindrical surfaces, or the Berezinskii-Kosterlitz-Thouless phase transition in a new geometry, perhaps also of supersolidity in crystalline single helium layers of variable density as predicted by Gordillo et al.[11].

Recent advances in nanomechanics have already allowed studies of liquids at small scales [12–16] but the study of the adsorption of superfluid helium on a single carbon nanotube is original (Fig. 1a). We fabricate mechanical resonators by suspending a single NT of 3 nm diameter and 1.1 μm length. This NT is contacted to two platinum electrodes and is capacitively coupled to a gate electrode (Fig. 1b). In order to suppress any surface contamination, we grow the nanotube in the last step of the fabrication process and we anneal it by passing a large current (6 μA) through it in the dilution refrigerator at 20 mK prior to the adsorption of helium. This procedure already allowed us to grow xenon monolayer crystals that were commensurate with the nanotube lattice [10]. The nanotube vibrates as a doubly-clamped string. The mechanical vibrations of the fundamental mode of the nanotube

are driven capacitively and measured electrically (Fig. 1c) [17–19]. The resonance frequency can be tuned by a large amount around 30 MHz when tuning the gate voltage (Figs. 1c and 1d). The quality factor deduced from the thermal motion linewidth is $\approx 2 \cdot 10^5$. We inject ^4He from room temperature into the sample cell through a capillary.

A mechanical resonator based on a suspended nanotube is a remarkable sensor of atoms adsorbed on its surface [20–23]. The mass detection can reach single atom resolution [20]. Driving the resonator to detect adsorbed atoms does not affect the dynamics of the adsorbates, since the amplitude of the driven vibrations can be kept smaller than the amplitude of thermal vibrations. The resonance frequency $f_0 = \frac{1}{2\pi} \sqrt{\frac{K}{M}}$ depends on the ratio of the string elasticity also called spring coefficient K to the effective mass M . The coefficient $K = k_{\text{NT}} + k_{\text{He}}$ is the sum of the respective elasticities of the naked NT- also called pristine - and of the adsorbed helium. Similarly the total mass $M = m_{\text{NT}} + m_{\text{He}}$ is the sum of the respective masses of the NT and of the adsorbed helium. With helium adsorbed, both K and M increase but their contributions to the resonance frequency have opposite signs, so that we could distinguish between them by varying the gate voltage. This is a great advantage of our experiment. Previous studies of two-dimensional helium superfluids often used torsional oscillators [4, 5, 24]. Contrary to our case, these torsional oscillators were macroscopic with not much possibility to change their resonance frequency so that mass effects were difficult to distinguish from elasticity effects [25]. As we shall see below, we have observed the two effects in two different temperature regimes.

By studying the transport properties of electrons inside the NT, we have demonstrated that our nanotubes are free of disorder. As a function of the gate voltage, the conductance is periodically modulated due to quantum electron interference [26]. This periodic modulation would be deteriorated by a tiny amount of disorder (see section I of Supplementary Information).

We measured the nanotube length $L \simeq 1.1 \mu\text{m}$ from the characteristic source-drain voltage $V_C = 1.5 \text{ mV}$ of the electron interference pattern. This length is $L = hv_F/2eV_C$ [26] where $v_F = 8 \times 10^5 \text{ m/s}$ is the Fermi velocity of nanotubes. It is consistent with the width of the trench and we obtained a similar but less reliable length ($L \approx 1 \mu\text{m}$) from the Coulomb blockade measurements of the conductance.

We observe a series of steps when measuring the resonance frequency of the nanotube as a function of the number N_{He} of helium atoms injected into the sample chamber (Fig. 1e). We

proceed by successive injections of $\approx 76 \text{ cm}^3$ of helium gas at a pressure set between 0.08 and 3 mbar. When we increase N_{He} , the vapour pressure P in the surrounding of the nanotube gets larger, but P cannot be quantitatively estimated due to the unknown adsorption of helium atoms onto the cell walls. We attribute the reduction of the resonance frequency Δf_0 measured in Fig. 1e to the helium mass m_{He} adsorbed on the NT. Each plateau in f_0 is assigned to a different layer adsorbed on the nanotube. At the completion of each layer, a new layer starts and the resonance frequency jumps down. It means a divergence of the coverage at constant helium pressure, that is, a divergence of the compressibility and a vanishing of the sound speed in the helium layer. This is in agreement with the first-order transition predicted for the layering transition [6]. The helium density at each discontinuity agrees within 6 % with the established density of helium adsorbed on graphite (Section III of Supplementary Information). During the completion of each layer, helium atoms must be homogeneously distributed over the surface and the chemical potential of the helium vapor needs to increase to equilibrate the increase of the repulsion between atoms. This explains the observed finite slope $\partial f_0 / \partial N_{\text{He}}$ of the plateaus (Fig. 1e).

Figure 2a shows the layer-by-layer desorption of helium from the surface of the nanotube, but now as a function of temperature up to 10 K and for 5 successive amounts of helium in the cell. The frequency of the steps are similar to those measured while varying N_{He} at constant temperature (Fig. 1e). One temperature sweep takes a few days to ensure the reproducibility of measurements. The layering transitions are rounded, probably because the layering transitions have a critical point of order 1 K (see Ref. [27]). By varying the gate voltage, consequently the spring constant, we have confirmed that the variation of the resonance frequency f_0 in Fig. 2a is due to the change in the resonator mass. Indeed the large frequency change Δf_0 is an increasing function of f_0 (Fig. 2b and Supplementary Section IV).

The first and second layers show some peculiar structures which would need further study to be compared with predictions by Boronat et al. (see Ref. [28] and Section VI of Supplementary Information). We thus focus on the third and fourth layers. By looking more precisely at the frequency variation below 0.7 K, we discovered the existence of a small minimum near 0.5 K (see Fig. 2c). The rise of f_0 above ~ 0.5 K in Fig. 2c signals the desorption of helium atoms from the nanotube. Figure 2d shows the dependence of the depth δf_0 of this small minimum on the gate voltage. Contrary to the case of the large

frequency shift Δf_0 of Fig. 2b, the slope is negative (see Fig. 2d and Supplementary Section IV). It means that this small minimum is due the helium contribution to the total spring constant of the resonator.

We attribute it to the temperature variation of the helium surface tension, that is, to the growing entropy of the helium film [29]. It is due to the third sound states in the case of thin superfluid films [30]. These waves are predicted to be longitudinal with no sizeable displacement of helium atoms in the direction perpendicular to the surface, except for densities near the layering transition [31]. The third sound has a linear energy dispersion given by the speed c . The resulting dependence of δf_0 on temperature T is

$$\delta f_0(T) = -0.074 \frac{1}{m_{\text{NT}} f_0} \frac{r_{\text{He}} (k_{\text{B}} T)^3}{L (\hbar c)^2} \quad (1)$$

where m_{NT} is the mass of the pristine nanotube, L the suspended nanotube length, k_{B} the Boltzmann constant, and \hbar the reduced Planck constant. See Section V of the Supplementary Information for a detailed derivation.

Figures 3b and 3e show a very good agreement with the T^3 law of Eq. (1) from which we could extract the sound velocity c (Figs. 3c and f). The layer fraction are computed by comparing the resonance frequency at 20 mK to the frequency of the jump indicated by the dashed line on Fig. 1e. We notice a large jump in sound velocity from the end of the 3rd layer (30 m/s) to the beginning of the 4th layer (210 m/s), in agreement with the predictions of a first order transition by Clements et al. [6, 7]. Although we found no evidence of ripplon excitations in our system, studying thicker helium layers may lead to their observation in future work.

Our work shows that helium layers adsorbed on carbon nanotubes are of unprecedented quality. This system is of great interest for the study of different quantum phenomena. The cylindrical boundary condition of the superfluid imposes quantized translational velocities of a vortex around the circumference [32]. This boundary condition also modifies the vortex-vortex interaction energy [32], so that it might alter the Berezinskii-Kosterlitz-Thouless topological phase transition. According to Gordillo et al. [11], helium monolayers adsorbed on nanotubes may become supersolid at low temperature. In summary, carbon nanotubes could be used for original studies of helium-based quantum phenomena.

Acknowledgments We thank N. Guenther, P. Massignan, A. Fetter, and G. A. Williams for fruitful discussions. This work is supported by the ERC advanced grant 692876, the

Foundation Cellex, the CERCA Programme, AGAUR, Severo Ochoa (SEV-2015-0522), the grant FIS2015-69831-P of MINECO, and the Fondo Europeo de Desarrollo Regional (FEDER). M.C.G. acknowledges partial financial support from the MINECO (Spanish Ministry of Economy) Grant No. FIS2017-84114-C2-2-P. M.C.G. also acknowledges the use of the C3UPO computer facilities at the Universidad Pablo de Olavide. J.B. acknowledges financial support from MINECO Grants FIS2014-56257-C2-1-P and FIS2017-84114-C2-1-P.

References

- [1] G. Zimmerli, G. Mistura, M. H. W. Chan, *Phys. Rev. Lett.* **68**, 60 (1992).
- [2] D.S. Greywall and P.A. Bush, *Phys. Rev. Lett.* **67**, 3535 (1991).
- [3] D.S. Greywall, *Phys. Rev. B* **47**, 309 (1993).
- [4] P. A. Crowell, J. D. Reppy, *Phys. Rev. B* **53**, 2701 (1996).
- [5] J. Nyéki, A. Phillis, A. Ho, D. Lee, P. Coleman, J. Parpia, B. Cowan, J. Saunders, *Nature Phys.* **13**, 455 (2017).
- [6] W. M. Saslow, G. Agnolet, C. E. Campbell, B. E. Clements, E. Krotscheck, *Phys. Rev. B* **54**, 6532 (1996).
- [7] B. E. Clements, E. Krotscheck, H. J. Lauter, *Phys. Rev. Lett.* **70**, 1287 (1993).
- [8] H. Godfrin, H.-J. Lauter, *Progress in Low Temp. Phys.* **14**, 213 (1995).
- [9] E. Menachekanian, V. Iaia, M. Fan, J. Chen, C. Hu, V. Mittal, G. Liu, R. Reyes, F. Wen, G. A. Williams *Phys. Rev. B* **99**, 064503 (2019).
- [10] A. Tavernarakis, J. Chaste, A. Eichler, G. Ceballos, M. C. Gordillo, J. Boronat, A. Bachtold *Phys. Rev. Lett.* **112**, 196103 (2014).
- [11] M. C. Gordillo, C. Cazorla, J. Boronat, *Phys. Rev. B* **83**, 121406 (2011).
- [12] E. Gil-Santos, C. Baker, D. T. Nguyen, W. Hease, C. Gomez, A. Lemaître, S. Ducci, G. Leo, I. Favero, *Nature Nanotechnol.* **10**, 810 (2015).
- [13] A. D. Kashkanova, A. B. Shkarin, C. D. Brown, N. E. Flowers-Jacobs, L. Childress, S. W. Hoch, L. Hohmann, K. Ott, J. Reichel, J. G. E. Harris, *Nature Phys.* **13**, 74 (2017).
- [14] S. Kaminski, L. L. Martin, S. Maayani, T. Carmon, *Nature Photon.* **10**, 758 (2016).

- [15] G. I. Harris, D. L. McAuslan, E. Sheridan, Y. Sachkou, C. Baker, W. P. Bowen, *Nature Phys.* **12**, 788 (2016).
- [16] D. L. McAuslan, G. I. Harris, C. Baker, Y. Sachkou, X. He, E. Sheridan, W. P. Bowen, *Phys. Rev. X* **6**, 021012 (2016).
- [17] V. Sazonova, Y. Yaish, H. Üstünel, D. Roundy, T. A. Arias, P. L. McEuen. *Nature* **431**, 284 (2004).
- [18] J. Moser, A. Eichler, J. Güttinger, M. I. Dykman, A. Bachtold, *Nature Nanotechnol.* **9**, 1007 (2014).
- [19] S. L. de Bonis, C. Urgell, W. Yang, C. Samanta, A. Noury, J. Vergara-Cruz, Q. Dong, Y. Jin, Y., A. Bachtold, *Nano Lett.*, **18**, 5324 (2018).
- [20] J. Chaste, A. Eichler, J. Moser, G. Ceballos, R. Rurali, A. Bachtold, *Nature Nanotechnol.* **7**, 301 (2012).
- [21] H.-Y. Chiu, P. Hung, H. W. Ch. Postma, M. Bockrath, *Nano Lett.* **8**, 4342 (2008).
- [22] Z. Wang, J. Wei, P. Morse, J. G. Dash, O. E. Vilches, D. H. Cobden, *Science* **327**, 552 (2010).
- [23] H.-C. Lee, O. E. Vilches, Z. Wang, E. Fredrickson, P. Morse, R. Roy, B. Dzyubenko, D. H. Cobden, *J. Low Temp. Phys.* **169**, 338 (2012).
- [24] D. J. Bishop, J. D. Reppy, *Phys. Rev. Lett.* **40**, 1727 (1978).
- [25] X. Mi and J. D. Reppy, *J. Low Temp. Phys.* **175**, 104 (2014).
- [26] W. Liang, M. Bockrath, D. Bozovic, J. H. Hafner, M. Tinkham, H. Park, *Nature* **411**, 665 (2001).
- [27] S. Ramesh, Q. Zhang, G. Torzo, J. D. Maynard, *Phys. Rev. Lett.* **52**, 2375 (1984).
- [28] M. C. Gordillo, J. Boronat, *Phys. Rev. B* **86**, 165409 (2012).
- [29] K. R. Atkins, Y. Narahara, *Phys. Rev.* **138**, A437 (1965).
- [30] K. R. Atkins, *Phys. Rev.* **113**, 962 (1959).
- [31] B. E. Clements, H. Forbert, E. Krotscheck, H. J. Lauter, M. Saarela, C. J. Tymczak *Phys. Rev. B* **50**, 6958 (1994).
- [32] N.-E. Guenther, P. Massignan, A. L. Fetter, *Phys. Rev. A* **96**, 063608 (2017).

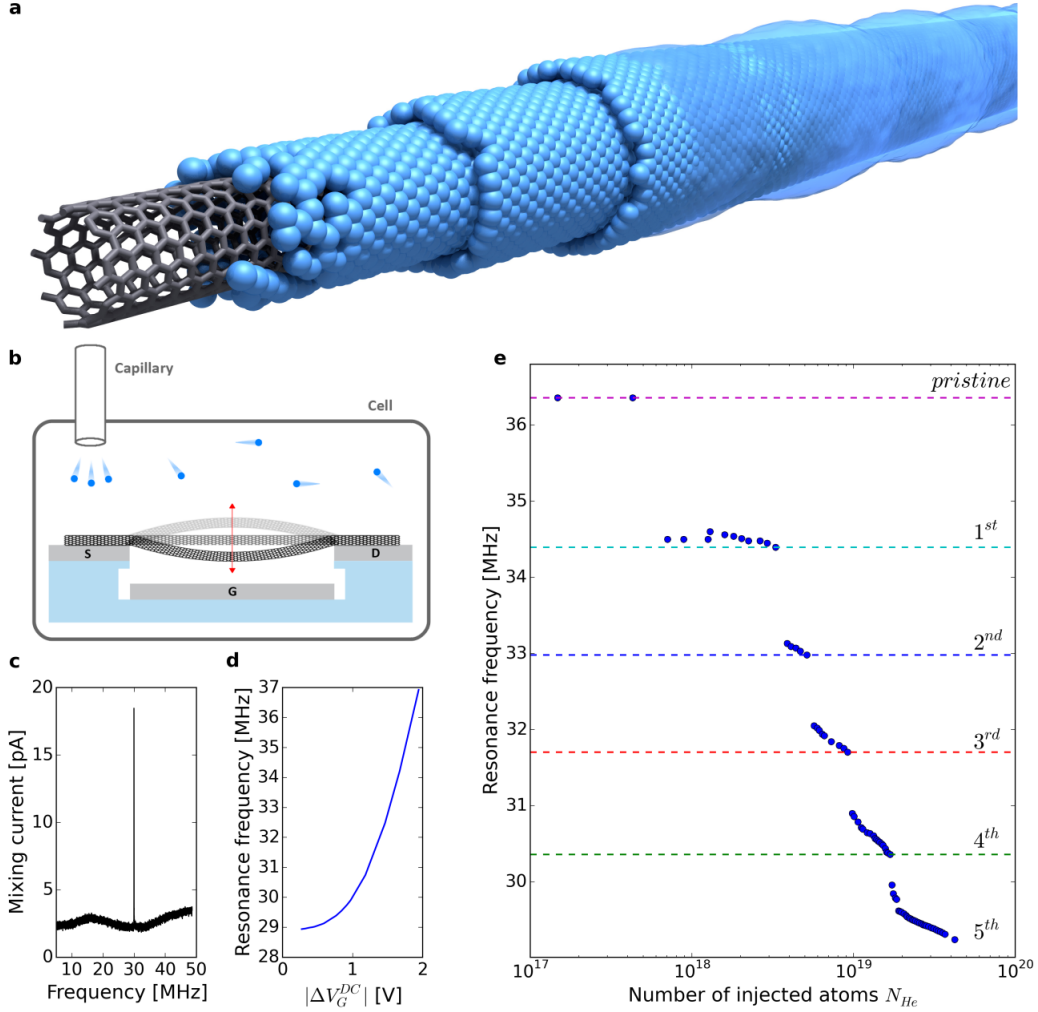


FIG. 1: **Helium multilayer adsorbed on a nanotube.** (a) Graphical representation of the helium multilayer on the nanotube. (b) Schematic of the nanotube mechanical resonator immersed in helium vapour. The nanotube is contacted to the platinum electrodes S and D and is capacitively coupled to the electrode G . (c) Spectrum of the mechanical vibration amplitude as a function of the drive frequency at 0.1 K and $V_G = 1.908$ V. (d) Gate voltage dependence of the resonance frequency. The offset due to the work function difference between the nanotube and the gate electrode is $V_G = 0.077$ V. (e) Layer-by-layer growth of the helium film. The resonance frequency is measured at 20 mK as a function of the number of helium atoms injected at room temperature into the cell through the capillary. The different steps are associated to the pristine nanotube and the successive adsorption of helium layers; the steps are labeled accordingly and highlighted by the horizontal dashed lines.

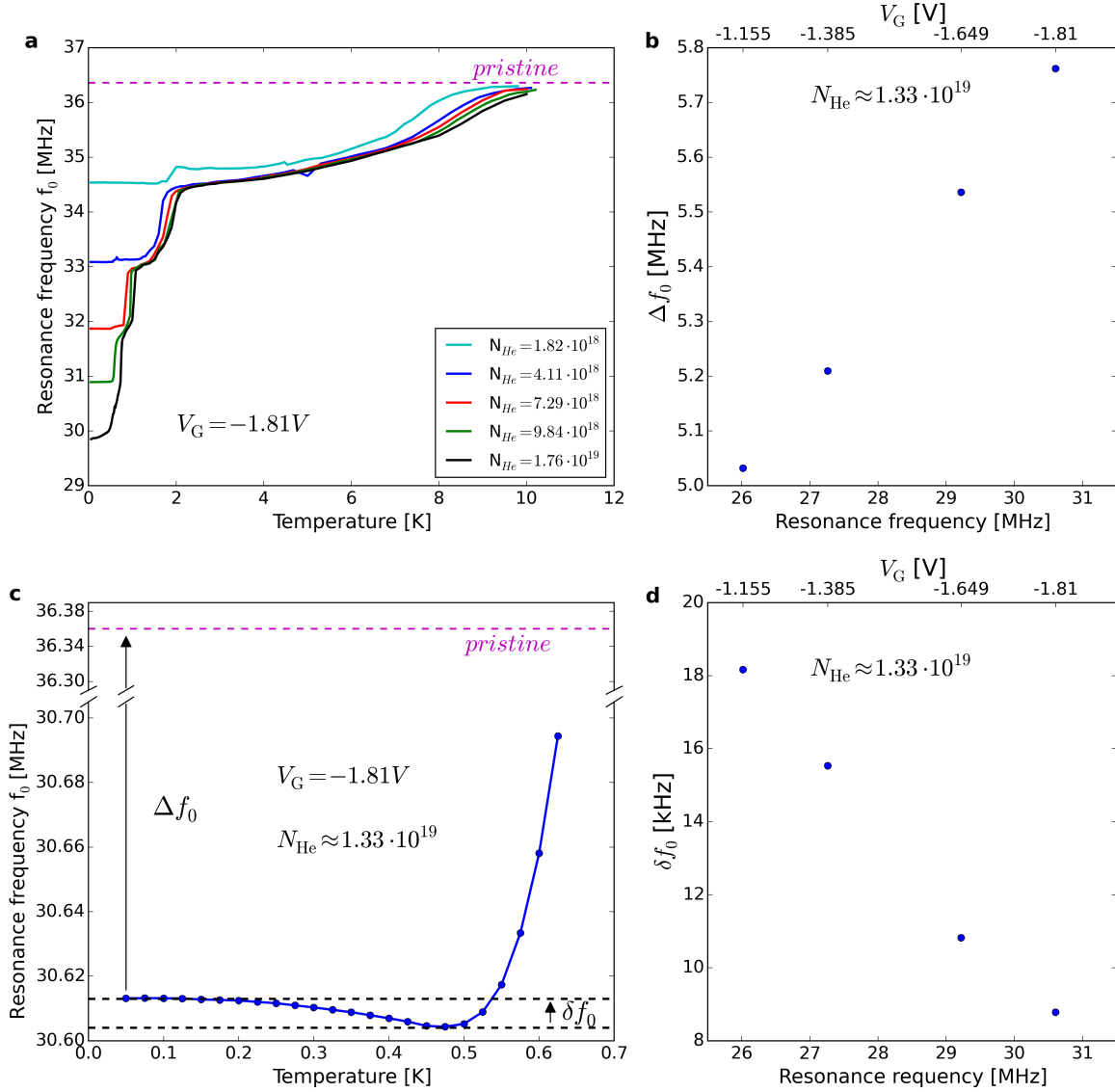


FIG. 2: **Layer-by-layer desorption upon increasing temperature.** (a) Resonance frequency as a function of temperature. The "pristine" is the carbon nanotube without any adsorption. (b) Frequency shift Δf_0 related to m_{He} as a function of gate voltage (upper axis) and resonance frequency (lower axis). As indicated in c, Δf_0 is the change in resonance frequency between the pristine nanotube and the dressed nanotube at 20 mK. (c) Temperature dependence of the resonance frequency in the low-temperature regime. (d) Frequency shift δf_0 related to k_{He} as a function of gate voltage (upper axis) and resonance frequency (lower axis). The shift δf_0 is represented in c.

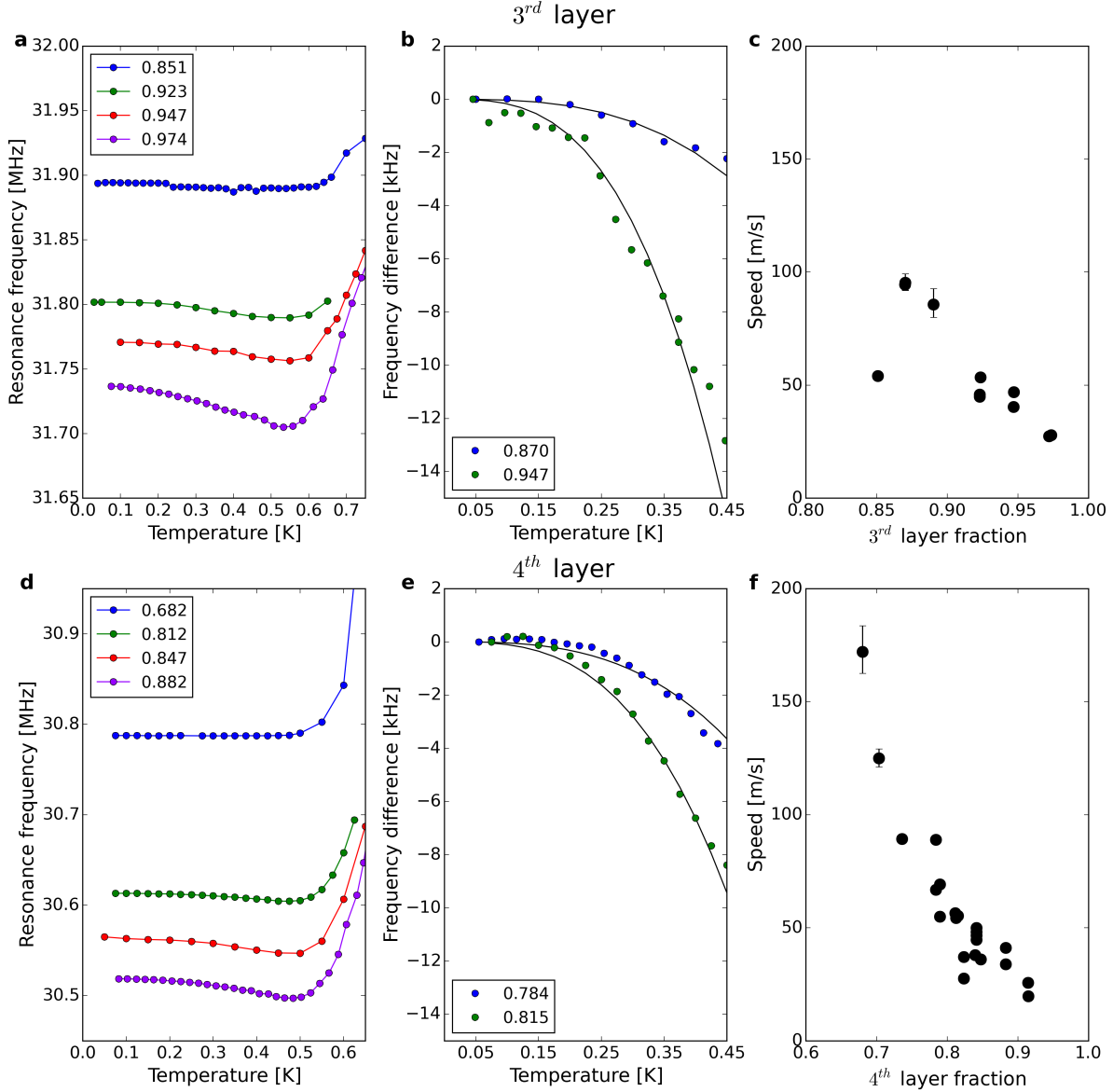


FIG. 3: **Mechanical sensing of the third sound.** (a) Resonance frequency as a function of temperature in the low-temperature regime for the third layer. The different curves correspond to different layer filling fractions, which are indicated in the legend. (b) Measured temperature dependence of the resonance shift (dots). The lines are cubic temperature dependencies, as expected from Eq. 1. (c) Third sound speed as a function of the layer filling fraction of the third layer. The error bars are obtained from the comparison between the measured $\delta f_0(T)$ dependence and Eq. 1. (d-f) Same as a-c but for the fourth layer.

Supplementary Information

Layering transition in superfluid helium adsorbed on a carbon nanotube mechanical resonator

Adrien Noury, Jorge Vergara-Cruz, Pascal Morfin, Bernard Plaçais, Maria C. Gordillo, Jordi Boronat, Sébastien Balibar, and Adrian Bachtold

I. QUANTUM ELECTRON TRANSPORT MEASUREMENTS

Figure 1a shows that the electrical characteristics of the nanotube studied in this work is typical of ultraclean nanotubes [1]. Near $V_G^{\text{DC}} = 0$ V, the conductance is suppressed to zero due to the small energy gap of the nanotube [2]. For positive V_G^{DC} values, $p-n$ junctions are formed near the metal electrodes. It creates Coulomb blockade peaks in the conductance (Fig. 1b). For negative V_G^{DC} , the nanotube is p -doped along the whole tube, resulting in a larger conductance approaching the quantum conductance $4e^2/h$ of small-gap nanotubes. In this regime, the conductance is modulated due to quantum electron interference [3]. Here, e is the charge of the electron and h is the Planck constant.

Figure 1c demonstrates that the nanotube is of high quality, since the modulation of the conductance is periodic over a large range of V_G^{DC} , and since this periodic modulation due to electron interference would be deteriorated by a tiny amount of disorder.

We quantify the nanotube length $L = 1.1 \mu\text{m}$ from the characteristic voltage bias $V_C = 1.5$ mV of the electron interference pattern shown in Fig. 1c using $L = hv_F/2eV_C$ [3]. Here, $v_F = 8 \times 10^5$ m/s is the Fermi velocity of nanotubes. This length is consistent with the width of the trench. We also obtain a similar length from the Coulomb blockade measurements in Fig. 1b. From the separation $\Delta V_G^{\text{DC}} = 18$ mV between two conductance peaks, we obtain the nanotube-gate capacitance $C_G = e/\Delta V_G^{\text{DC}} = 8.9 \times 10^{-18}$ F. We get the length $L \simeq 1 \mu\text{m}$ of the suspended nanotube using

$$C_G = \frac{2\pi\epsilon_0 L}{\ln\left(\frac{2d}{r}\right)}, \quad (1)$$

where ϵ_0 is the vacuum permittivity, $d = 350$ nm the separation between the nanotube and the gate electrode, and r the nanotube radius. This estimation of the length is less reliable than the previous one because Eq. 1 does not take into account the screening of the electric

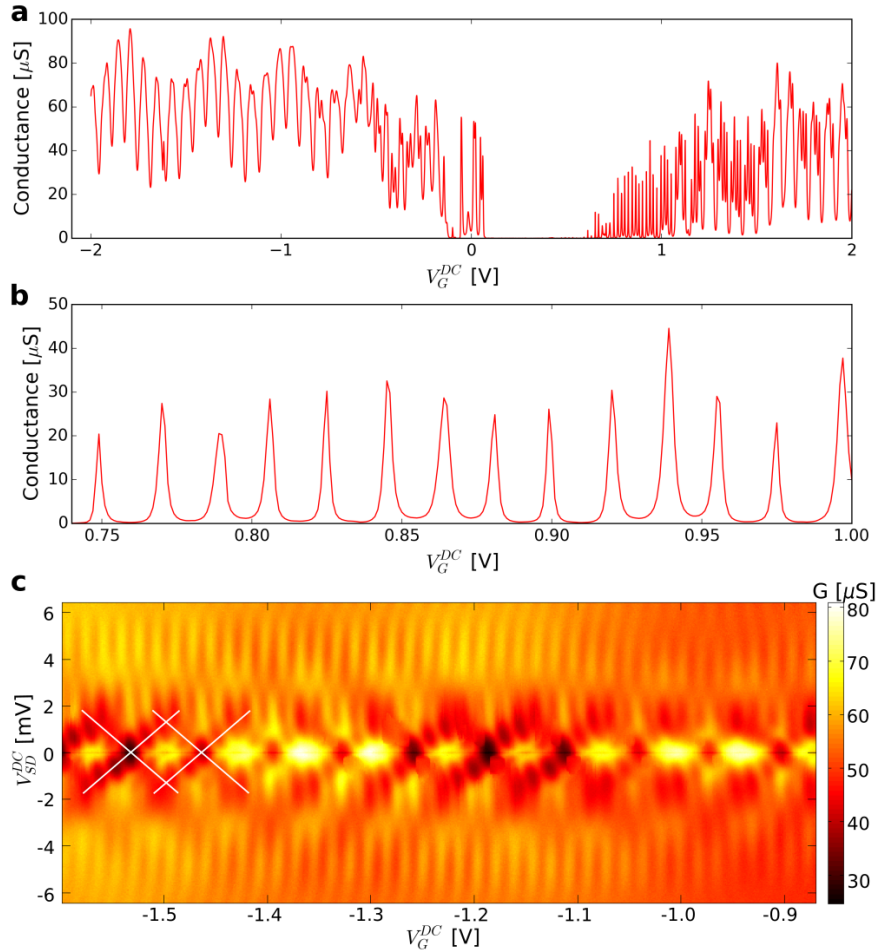


FIG. 1. **Electron transport measurements of the nanotube discussed in the main text.** (a,b) Conductance of the nanotube as a function of gate voltage measured at the base temperature of the cryostat over two different gate voltage ranges. (c) Differential conductance as a function of $V_{\text{SD}}^{\text{DC}}$ and V_G^{DC} at the base temperature of the cryostat. The intersection of the white lines at $V_G = 1.5$ mV corresponds to the characteristic voltage bias of the electron interference

field between the nanotube and the gate electrode by the source and the drain electrodes.

II. TRANSDUCTION OF DISPLACEMENT INTO CURRENT

We measure the mechanical vibrations of the nanotube with the two-source technique [4, 5]. Displacement modulations result in current modulations by applying an input oscillating

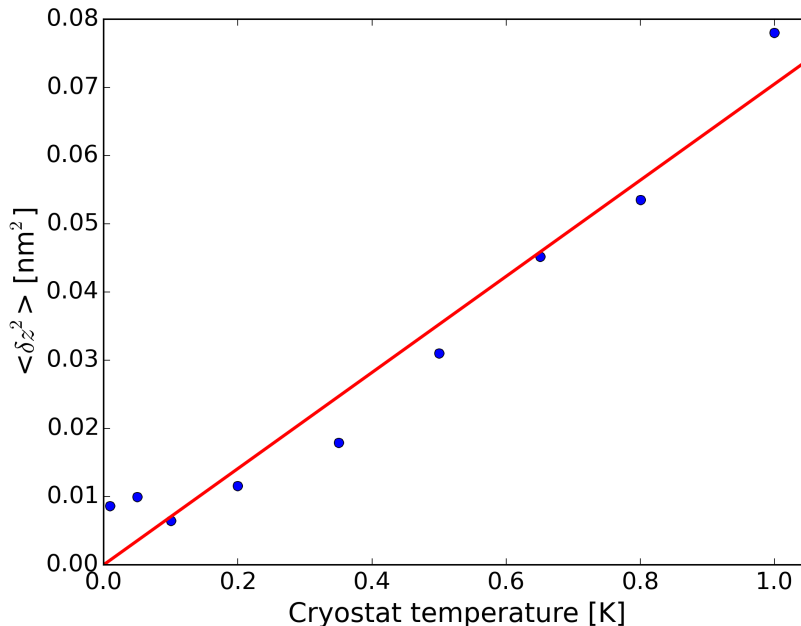


FIG. 2. **Variance of the mechanical displacement as a function of temperature.** Measurements are carried out on the nanotube discussed in the main text.

voltage with amplitude $V_{\text{SD}}^{\text{AC}}$ across the nanotube. We assume that the resonance used in the measurements of the main text corresponds to the fundamental eigenmode polarized in the direction perpendicular to the surface of the gate electrode, which is a good assumption since the signal of the driven vibrations of this resonance is much larger than the signal of the other resonances. The current δI at the frequency close to the difference between the mode eigenfrequency and the frequency of the source-drain voltage is

$$\delta I = \beta \delta z, \quad (2)$$

$$\beta = \frac{1}{2} \frac{dG}{dV_G} V_G^{\text{DC}} V_{\text{SD}}^{\text{AC}} \frac{C'_G}{C_G}. \quad (3)$$

Here, δz is the displacement of the nanotube, dG/dV_G is the derivative of the conductance with respect to the gate voltage, V_G^{DC} is the static gate voltage, and C'_G is the derivative of C_G with respect to z . We quantify $C'_G = 4.1 \times 10^{-12}$ F/m using the relation $C'_G = \frac{C_G}{d \ln(2d/r)}$.

We estimate the effective mass $m = 3.5$ ag from the measurement of the variance of the displacement noise $\langle \delta z^2 \rangle$ as a function of temperature T (Fig. 2). The displacement noise of the nanotube is measured with the electrical method described in Ref. [5] and using Eqs. 2 and 3. We compare the measured slope of $\langle \delta z^2 \rangle$ as a function of T to the slope expected

from the equipartition theorem, which reads $m\omega_0^2\langle\delta z^2\rangle = k_b T$. Here, $\omega_0/2\pi$ is the resonance frequency of the eigenmode and k_b is the Boltzmann constant. This mass is consistent with the mass of a $\sim 1.1 \mu\text{m}$ long nanotube.

We evaluate the nanotube radius $r \simeq 1.5 \text{ nm}$ from the effective mass using the relation

$$m = \frac{1}{2} \left(2m_C \times \frac{2\pi r \times L}{A_h} \right), \quad (4)$$

where $m_C = 2 \times 10^{-26} \text{ kg}$ is the mass of a carbon atom and $A_h = 5.2 \times 10^{-20} \text{ m}^2$ is the surface area of a hexagon in the honeycomb lattice of graphene. The coefficient $\frac{1}{2}$ on the right-hand side of Eq. 4 comes from the normalisation of the mass of the resonator due to the shape of the eigenmode. We assume here that the modal shape is $\phi(x) = \cos(\pi x/L)$, a good approximation for the shape of a beam under tension.

III. DENSITY OF HELIUM LAYERS

We can reliably quantify the ratio between the number N_{He} of adsorbed helium atoms and the number N_C of carbon atoms at the surface of the nanotube from the measurement of the resonance frequency [6, 7]. This ratio, called coverage, reads

$$\phi = \frac{N_{\text{He}}}{N_C} = \frac{m_C}{m_{\text{He}}} \left[\left(\frac{f_0^{\text{NT}}}{f_0^{\text{NT+He}}} \right)^2 - 1 \right], \quad (5)$$

where m_C and m_{He} are the atomic masses of carbon and helium atoms, respectively. Here, $f_0^{\text{NT+He}}$ is the resonance frequency of the nanotube covered by helium atoms, and f_0^{NT} is

		Areal density (atoms/nm ²)	
	f_0 (MHz)	nanotube	graphite
Pristine substrate	36.34	0	0
First layer completed	34.41	11.0	11.4
Second layer completed	32.97	8.1	8.6
Third layer completed	31.69	7.2	7.6
Fourth layer completed	30.39	7.3	7.6

TABLE I. Areal density of completed helium layers on the nanotube. The density of helium adsorbed on graphite is also shown [8].

the resonance frequency of the pristine nanotube without any adsorbed helium atoms. The coverage of noble gas atoms adsorbed on nanotube resonators can be successfully quantified with Eq. 5 because these adsorbed atoms increase the mass of the resonator but do not modify its spring constant [6, 7]. Indeed, the interaction between noble gas atoms is much weaker than that between the carbon atoms of the nanotube.

Table I shows the areal density of the different completed helium layers. The areal density is estimated from the coverage and taking into account the cylindrical geometry that normalizes the density by the factor $\frac{r}{r+i \cdot d_1}$. Here, r is the nanotube radius, i is the layer number, and d_1 is the layer-layer separation. The characterisation of the nanotube in the previous section indicates that $r = 1.5$ nm. The separation between layers is taken equal to $d_1 = 0.27$ nm, the separation between the first helium layer and graphite [9]. Table I shows that the estimated areal densities are remarkably close to the values measured with helium adsorbed on graphite [8].

IV. RESONANCE FREQUENCY SHIFT – A MASS EFFECT OR A SPRING EFFECT?

We look at the f_0 dependence of two different frequency shifts, namely Δf_0 and δf_0 (see Fig. 2 in the article), which show opposite behavior. The resonance frequency of the nanotube covered by helium depends on three parameters: the helium pressure in the cell P_{He} , the temperature T , and the gate voltage V_G^{DC} . The resonance frequency of the bare nanotube depends only on the DC gate voltage V_G^{DC} as

$$f_0(V_G^{\text{DC}}) = \frac{1}{2\pi} \sqrt{\frac{k_{\text{NT}}(V_G^{\text{DC}})}{m_{\text{NT}}}}, \quad (6)$$

where the nanotube stiffness k_{NT} can be changed by tuning the gate-voltage V_G^{DC} , in contrast to the nanotube mass m_{NT} . We measure that $f_0(V_G^{\text{DC}})$ is temperature independent at a fixed V_G^{DC} . Straining the nanotube with gate voltage is very efficient, since $f_0(V_G^{\text{DC}})$ can be varied by $\sim 16\%$ in Figs. 2b and 2d of the article. Due to the large nanotube stiffness, the longitudinal deformation of the nanotube is minute and the helium film structure also. Furthermore, the surface density of helium on the nanotube is fixed by the temperature and the helium pressure in the cell.

The resonance frequency of the nanotube coated by a thin helium film is:

$$f_1 = \frac{1}{2\pi} \sqrt{\frac{k_{NT} + k_{He}}{m_{NT} + m_{He}}} \approx f_0 \left(1 - \frac{m_{He}}{2m_{NT}} + \frac{k_{He}}{2k_{NT}}\right) \quad (7)$$

High-frequency nanotube mechanical resonators are highly sensitive to helium coating. Loading the nanotube with a single helium layer gives rise to a mass increment $m_{He}/m_{NT} \lesssim 10\%$ and a decrease of the resonance frequency $(f_1 - f_0)/f_0 \approx -m_{He}/2m_{NT} \lesssim -5\%$. A second effect of the helium coverage is the modification of the nanotube spring constant due to a modification of the surface tension. The effect is extremely small because of the weak He-He interaction compared to the covalent C-C interaction, but still measurable thanks to the remarkable sensitivity of high-Q nanotube resonators. By studying the V_G^{DC} dependence of the frequency shifts, it is possible to distinguish the two contributions. Indeed, as a function of the helium pressure and the temperature, the frequency shift is expressed as

$$f_0 - f_1 \approx f_0(V_G^{DC}) \left(\frac{m_{He}(P_{He}, T)}{2m_{NT}} - \frac{k_{He}(P_{He}, T)}{2k_{NT}(V_G^{DC})} \right), \quad (8)$$

$$f_0 - f_1 \approx \left(\frac{1}{2m_{NT}} \right) \left(f_0(V_G^{DC}) \times m_{He}(P_{He}, T) - \frac{k_{He}(P_{He}, T)}{4\pi^2 f_0(V_G^{DC})} \right). \quad (9)$$

Mass effects increase proportionally to f_0 whereas stiffness effects decrease proportionally to $(1/f_0)$. The former depends on the adsorbed helium mass, consequently on the gas pressure, on temperature, possibly also on changes in superfluid mass fraction. The later addresses the physics of the helium surface tension which carries additional signatures of the layering transition. Note that a V_G^{DC} -dependence of k_{He} and m_{He} would intervene as a second order correction in the developments, which justifies the above variable separation.

Let us now look at the f_0 dependence of the frequency shift Δf_0 that is indicated on Fig. 2c of the article. We expect it to be a mass effect due to the helium evaporation between 10 mK and 10K so that Δf_0 should obey the equation:

$$\Delta f_0 \approx \frac{f_0(V_G^{DC})m_{He}(P_{He}, 10 \text{ mK})}{2m_{NT}}. \quad (10)$$

Δf_0 should be an increasing function of f_0 , in agreement with the measurements on Fig. 2b of the article.

On the opposite, Fig. 2d of the article shows that δf_0 is a decreasing function of f_0 which demonstrates that this slight frequency dip is due to some change in the elastic constant k_{He} . Indeed it writes now:

$$\delta f_0 \approx -\frac{\delta k_{He}(P_{He})}{8\pi^2 m_{NT} f_0(V_G^{DC})} \quad (11)$$

where δk_{He} is the change in the helium surface tension from 10 mK to the temperature of the minimum (about 0.5K, see Fig. 2c of the article). Here, δk_{He} is negative and we attribute it to the increasing entropy of the helium film. In this case, one expects that δf_0 decreases with f_0 , which is confirmed by our measurements (see Fig. 2d of the article). We cannot attribute it to some superfluid-normal transition in the film because this would be a mass effect with the opposite dependence on f_0 . As shown in the next section, we have calculated the temperature dependence of the helium surface tension, which can describe our measurements.

V. SURFACE TENSION – THERMALLY EXCITED THIRD SOUND STATES

We show in the main text that the measured spring constant of the nanotube covered by superfluid helium is temperature dependent. In this section, we relate this observation to the change of the surface tension of the superfluid due to thermally excited third sound states.

The surface tension γ is the free energy of the superfluid surface per unit area. When varying the superfluid surface area by δA , the energy changes as

$$\delta E = \gamma \cdot \delta A. \quad (12)$$

The surface tension contributes to the spring constant of the resonator. Any small deviation from the equilibrium position of the superfluid leads to a spring force. The modulation δA is related to the modulation of the resonator length δl when the nanotube is vibrating. The modulation is $\delta A = 2\pi r_{\text{He}} \cdot \delta l$ where r_{He} is the radius of the surface of the helium superfluid covering the nanotube. In order to relate δl to the displacement δz of the nanotube resonator, we consider the fundamental mode of a doubly-clamped nanotube string. The transverse displacement of the resonator along its axis x is given by $Z(x, t) = \delta z(t) \cdot \phi(x) = \delta z(t) \cdot \cos(\pi x/L)$ with $\phi(\pm L/2) = 0$ the boundary conditions at the clamping points. When the nanotube moves by δz , the total length becomes

$$L + \delta l = \int_{-L/2}^{+L/2} dx \sqrt{1 + \left(\frac{\partial Z}{\partial x}\right)^2} \simeq L + \frac{1}{2} \int_{-L/2}^{+L/2} dx \left(\frac{\partial Z}{\partial x}\right)^2 = L + \frac{\pi^2}{4L} \delta z^2. \quad (13)$$

As a result, the energy associated to the surface tension of the superfluid film is the energy

of a harmonic oscillator $\delta E = \frac{1}{2}k_{\text{He}}\delta z^2$ with spring constant

$$k_{\text{He}} = \gamma\pi^3\frac{r_{\text{He}}}{L}. \quad (14)$$

The restoring force of the helium film acts in parallel to the restoring force of the pristine carbon nanotube k_{NT} , so that the total spring constant is $k_{\text{total}} = k_{\text{He}} + k_{\text{NT}}$. It is important to emphasize that the helium film contributes weakly to the total spring constant, since the interaction between noble gas atoms is 2 orders of magnitude weaker than that of covalent C-C bonds, as demonstrated experimentally in Refs. [6, 7]. For this reason, any change of the surface tension leads to a minuscule change of the resonance frequency of the resonator, as observed in our experiments discussed in the main text.

It is interesting to compare the typical elongation δl in our experiments with the separation between two helium atoms. The modulation of the elongation is small so that the number of helium atoms adsorbed on the suspended nanotube remains constant. Indeed, the amplitude of the thermal vibrations is ≤ 300 pm below $T = 1$ K so that the associated nanotube elongation is $\delta l \leq 0.2$ pm using Eq. 13. For comparison, the separation between helium atoms in thin films is typically 0.3 nm.

The temperature dependence of the surface tension arises from the change of the free energy of the superfluid, that is, from the thermal excitation of two-dimensional third sound states. To compute $\gamma(T)$, we follow the calculations of Atkins using third sound states instead of the surface tension waves in three-dimensional superfluid helium [10]. Below 1 K, the third sound dispersion is given by

$$\omega = ck \quad (15)$$

with the angular frequency ω , the superfluid velocity c , and the wavevector strength k [11]. In order to calculate the density of states, we first count the number N_{st} of states within the surface πk^2

$$N_{\text{st}} = \frac{L_0^2}{(2\pi)^2}\pi k^2 \quad (16)$$

with L_0^2 the surface area. The density of states is given by the number of states within the frequency $\delta\omega$ and per unit of surface,

$$\frac{g(\omega)\delta\omega}{L_0^2} = \frac{1}{L_0^2}\delta N_{\text{st}} = \frac{1}{L_0^2}\frac{dN_{\text{st}}}{dk}\left(\frac{d\omega}{dk}\right)^{-1}\delta\omega = \frac{\omega}{2\pi c^2}\delta\omega \quad (17)$$

The internal energy of thermally excited third wave states per unit surface is then

$$U_{\text{th}} = \int_0^\infty \frac{\hbar\omega}{\exp(\hbar\omega/k_{\text{B}}T) - 1} g(\omega) d\omega = \frac{1}{2\pi c^2} \frac{(k_{\text{B}}T)^3}{\hbar^2} \int_0^\infty \frac{x^2}{\exp(x) - 1} dx = 0.38 \frac{(k_{\text{B}}T)^3}{(\hbar c)^2}. \quad (18)$$

When the internal energy varies as $U \propto T^\lambda$, the free energy scales as $F = -\frac{1}{\lambda-1}U$ from simple thermodynamics [10]. As a result, the variation of the free energy per unit surface when increasing the temperature from 0 K is

$$\Delta\gamma(T) = U_{\text{th}} - TS = -\frac{1}{2}U_{\text{th}}. \quad (19)$$

Here, S is the entropy per unit surface. As a result, we obtain

$$\Delta\gamma(T) = -0.19 \frac{(k_{\text{B}}T)^3}{(\hbar c)^2}. \quad (20)$$

The change in free energy is related to the change in spring constant using Eq. 14

$$\delta k_{\text{He}}(T) = -5.89 \frac{r_{\text{He}}}{L} \frac{(k_{\text{B}}T)^3}{(\hbar c)^2}, \quad (21)$$

When increasing the temperature from 0 K, the resonance frequency f_0 of the nanotube string covered by the helium film is expected to decrease as

$$\delta f_0(T) = \frac{1}{2} \frac{\delta k_{\text{He}}(T)}{k_{\text{NT}}} f_0 = -0.074 \frac{1}{m_{\text{NT}} f_0} \frac{r_{\text{He}}}{L} \frac{(k_{\text{B}}T)^3}{(\hbar c)^2}. \quad (22)$$

VI. THEORETICAL CALCULATIONS

Figures 3a,b show the energy per ^4He atom as a function of density for the first and second layer, respectively. Calculations are performed using diffusion Monte Carlo method, as described in ref [12]. The calculations are performed for a nanotube radius of 1.43 nm.

On Fig. 3a is displayed the energy of atoms in both a liquid (red) and solid (blue) configuration when the nanotube is covered by one layer. The ground state of the system corresponds to a liquid of density $0.0432 \pm 0.003 \text{ \AA}^{-2}$. From a density of $0.087 \pm 0.005 \text{ \AA}^{-2}$ up, the solid structure is more stable than the liquid. We then conclude that at the second layer promotion (density of $\approx 0.12 \text{ \AA}^{-2}$) the first layer is solid. This is consistent with measurements and calculations on helium adsorbed on graphite [8, 13].

On Fig. 3b is displayed the energy of the atoms in the second layer. The ground state of the system always corresponds to a liquid. The result of these calculations is different

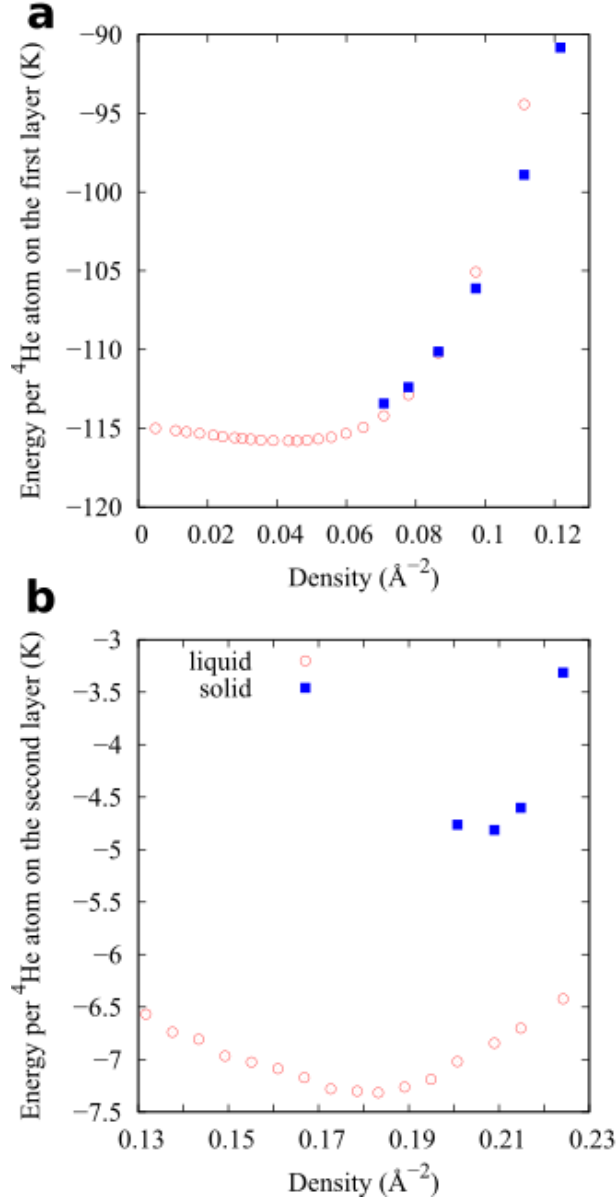


FIG. 3. Calculated energy per atom in the first layer and the second layer (a) First layer. (b) Second layer. Energy per atom for both a liquid (red circles) and a solid (blue squares).

from that of previous works on helium adsorbed on graphite, where the second layer at completion is solid [8, 13]. More work has to be carried out in order to be able to make a firm conclusion on the phase of the second layer adsorbed on nanotubes. For this, a more advanced model can be used in order to take into account for instance the corrugation of

the nanotube.

- [1] J. Moser, A. Eichler, J. Güttinger, M. I. Dykman, A. Bachtold, *Nature Nanotech.* **9**, 1007 (2014).
- [2] E. A. Laird, F. Kuemmeth, G. A. Steele, K. Grove-Rasmussen, J. Nygard, K. Flensberg, L. P. Kouwenhoven, *Rev. Mod. Phys.* **87**, 703 (2015).
- [3] W. Liang, M. Bockrath, D. Bozovic, J. H. Hafner, M. Tinkham, H. Park, *Nature* **411**, 665 (2001).
- [4] V. Sazonova, Y. Yaish, D. Üstünel, D. Roundy, T. A. Arias, P. L. McEuen, *Nature* **431**, 284 (2004).
- [5] S. L. de Bonis, C. Urgell, W. Yang, C. Samanta, A. Noury, J. Vergara-Cruz, Q. Dong, Y. Jin, Y., A. Bachtold, *Nano Lett.*, **18**, 5324 (2018).
- [6] Z. Wang, J. Wei, P. Morse, J. G. Dash, O. E. Vilches, D. H. Cobden, *Science*, **327**, 552 (2010).
- [7] A. Tavernarakis, J. Chaste, A. Eichler, G. Ceballos, M. C. Gordillo, J. Boronat, A. Bachtold, *Phys. Rev. Lett.*, **112**, 196103 (2014).
- [8] P. A. Crowell, J. D. Reppy, *Phys. Rev. B*, **53**, 2701 (1996).
- [9] P. Corboz, M. Boninsegni, L. Pollet, M. Troyer, *Phys. Rev. B*, **78**, 245414 (2008).
- [10] K. R. Atkins, *Can. J. Phys.*, **31**, 1165 (1953).
- [11] J. E. Rutledge, W. L. McMillan, J. M. Mochel, T. E. Washburn, *Phys. Rev. B*, **18**, 2155 (1978).
- [12] M. C. Gordillo, J. Boronat, *Phys. Rev. B*, **86**, 165409 (2012).
- [13] M. C. Gordillo, D. M. Ceperley, *Phys. Rev. B*, **58**, 6447 (1998).